Available online at www.sciencedirect.com
ScienceDirect
International Journal of Mechanical Sciences 50 (2008) 275–292
International Journal of MECHANICAL SCIENCES
www.elsevier.com/locate/ijmecsci

Exact full-field analysis of strain and displacement for circular disks subjected to partially distributed compressions

Chien-Ching Ma[a,*], Kuang-Ming Hung[b]

[a]Department of Mechanical Engineering, National Taiwan University, Taipei 10617, Taiwan, ROC
[b]Department of Mechanical Engineering, Hwa-Hsia Institute of Technology, Taipei County 23554, Taiwan, ROC

Received 30 November 2006; received in revised form 22 June 2007; accepted 22 June 2007
Available online 4 July 2007

Abstract

The disk in diametral compression has been investigated frequently on developing experimental techniques, such as photoelasticity and Moiré interferometry, for several decades. Theoretically, the compression as a concentrated force is more conducive to analyze but it is impossible to achieve such loading condition experimentally. The distributed compression on a finite area at rim is important in many engineering applications and is relatively closer to actual testing conditions, but it is complicated to seek an analytical solution. This paper presents exact full-field solutions of strain and displacement of a circular disk subjected to partially diametral distributed compressions in explicit functional forms. Based on the theoretical solutions, full-field distributions of strain and displacement are easily provided in polar and Cartesian coordinates by numerical calculations. Interesting phenomena of strain and displacement are discussed in detail based on numerical results. The Saint-Venant's principle applied in circular disks subjected to diametral loadings is examined by comparing the full-field results for the concentrated load and the distributed compression with small angle. Experimental measurements of full-field displacement contours and isochromatic fringe patterns are used to compare with the theoretical predictions and good agreements of both results are found.

Keywords: Plane problem; Circular disk; Partially distributed compression; Strain; Displacement

1. Introduction

An experimental test of a plane disk subjected to diametrically concentrated forces is known as the split cylinder or the Brazilian test. A bi-axial stress state is evolved (vertically compressive and horizontally tensile) and leads to the sample failing in tension at its centre. The split cylinder test is an extremely useful method for determining the tensile strength of concrete and other brittle materials that have much higher compressive strengths than tensile strength. Ideally, the tensile failure will occur along the loaded diameter, splitting the cylinder (or disk) into two halves [1]. A Brazilian scholar, professor Carneiro, was the inventor of the split tension test for measuring the tensile strength of concrete; it was for whom that the word Brazilian test was turned out. He observed that concrete fracture developed almost strictly in a vertical plane connecting the line of contact between the cylindrical specimen and the compression plates. This observation brought about the development of Brazilian test that could be performed on cylinders. Using simple formulas based on elasticity theory, Carnero evaluated the tensile strength from the elastic tensile strength limit. This method was presented at the meeting of the Brazilian Association for Technical Rules [2]. A similar method was independently presented in Japan by Akazawa [3] at almost the same time. Even since, the Brazilian test has been the subject of many studies all over the world. Fairbairn and Ulm [4] made a detailed description for the contribution of professor Carneiro on Brazilian test. The Brazilian test was also widely used to test tensile strength of rock and other brittle materials. Recent developments of

*Corresponding author. Tel.: +886 2 23659996; fax: +886 2 23631755.
E-mail address: ccma@ntu.edu.tw (C.-C. Ma).

0020-7403/$ - see front matter © 2007 Elsevier Ltd. All rights reserved.
doi:10.1016/j.ijmecsci.2007.06.005

Brazilian test include testing fracture toughness, elastic modulus, extending from isotropic to anisotropic materials [5,6]. Tensile strength of rock is among the most important parameters influencing rock deformability and crushing. To calculate the tensile strength from Brazilian test, one must know the principal tensile stress, in particular at the rock disk center, where a crack initiates. Disk compression tests have been employed to determine the fracture strength in graphite [7,8].

The theoretical investigation of a circular disk subjected to concentrated forces applied at its boundary is most frequently quoted in classical elasticity. Since the circular disk has very simple boundary conditions and geometry, it has been a classic problem since 1883, attracting the attention of many mathematicians. The stress analysis of the circular disk subjected to concentrated forces has been discussed by Frocht [9], Timoshenko and Goodier [10], Muskhelishvili [11], and Sokolnikoff [12]. Because the experiment of a disk in diametral compression is easy to employ and the analytical solution of full-field stress can be used as a theoretical reference to check experiment, the problem of a disk in diametral compression has certain contribution to many experimental stress analysis literatures for several decades. On surveying photoelastic development, Frocht [9] plots isochromatic/isoclinic fringes from the analytical solution of stress field and compared with experimental images. Pindera and Pindera [13] using the method of isodynes technique demonstrated experimental results of this problem based on carefully conducted experiments. Fairhurst [14] analyzed the failure in the Brazilian tensile test on the basis of a Griffith-type fracture criterion. Voloshin and Burger [15] brought up a half-fringe method to increase isochromatics. Brown and Sullivan [16] proposed a computer-aided holophotoelastic method to combine data obtained from three methods, which are phase-stepped holography, half-fringe photoelasticity, and polarization-stepped photoelasticity. Chen and Chen [17] used two-wavelength method and polarization-stepped method to separate isochromatics and isoclinics from digital photoelastic image. The diametrical compression or Brazilian disk test can be use to determine the mechanical properties of materials. With the established theoretical displacement fields of a circular disk subjected to concentrated forces, an inverse approach was implemented to determine material constants from the experimentally measured displacement fields using moiré fringes [18–20]. Model of disk in diametral compression has been quoted by all of these literatures mentioned above.

The classical theory assumed that the concentrated load is applied over an infinitesimally small width. A concentrated load is assumed to be applied as a theoretical line load, but clearly this would lead to stresses of very great intensity in the vicinity of the line of applied loading. Hence, the actual loads in experiment are not concentrated but distributed over finite portions of the disk. Brazilian test model is the most correspondent testing status for disk in diametral compression because the loading of disk is changed from the concentrated force to a distributed compression along two opposite directions facing each other on the rim. The distributed loading applied on a disk in diametral compression is more difficult to analyze than that of the concentrated force. Hondros [21] analyzed the problem in the Brazilian test for the case of a thin disk loaded by a uniform pressure, radially applied over a short strip of the circumference at each end of a diameter. He obtained the full-field stresses in series solutions by using the series expansion technique and applied these solutions to evaluate the Young's modulus and Poisson's ratio of concrete by measuring strain. Recently, Hung and Ma [22] continued and extended Hondros' work to successfully obtain the analytical solution in explicit form with simple expression instead of using series solution for full-field stresses, which can provide the full-field calculation capability as well as in depth theoretical basis. In addition, they also obtained concise mathematical forms for principal stress orientation and maximum shear stress. However, all the researches for the theoretical analysis of disks mentioned above are all focused on the solutions of stresses. There are only very few analytical results of the displacements available in the literature. Davison et al. [23] provided a general displacement-based elasticity solution for the problem of an arbitrarily layered disk subjected to distributed loadings. This solution technique extended the local/global stiffness matrix formulation for analyzing the multilayered problem in rectangular coordinates to non-axisymmetric polar problems by using Fourier series expansion technique. Because of the difficulty of the problem considered by Davison et al. [23], solutions of displacement were expressed in series forms.

The derivation of exact solutions for the deformation of disks subjected to distribute loadings is important in many engineering applications and it also provides useful information for the experimental measurement. This paper extends the work of Hung and Ma [22] to derive the exact analytical full-field solutions of strain and displacement for circular disks (plane stress) and cylinders (plane strain) subjected to partially diametral distributed compressions. These solutions include three in-plane strains and one normal strain (plane stress case) along the thickness direction, and two in-plane displacements and one out-of-plane displacement (plane stress case). This paper provides complete information of deformations for circular disks subjected to partially diametral distributed compressions and concentrated loads in a two-dimensional configuration. It is worthy to note that all the solutions obtained in this paper are expressed in explicit simple functional forms without integrations or summations; hence it is easy to be used as a theoretical reference to compare with the experimental results. The numerical calculations based on explicit simple theoretical solutions are very easy to perform without introducing any numerical errors. Full-field distributions of strain and displacement are provided by numerical calculations and are compared with experimental measurements of displacement contours and isochromatic fringe patterns. Good agreements of both results are found.

Saint-Venant's principle states that a system of forces acting over a small region of the boundary can be replaced by a statically equivalent system of forces without introducing appreciable changes in regions well removed from the area of

load application. The solution will be correct everywhere except for a small area near the boundary where the forces are applied. This area is dependent on the geometry of the specimen and the distribution of the loading. Detailed discussions from the full-field plots of strain and displacement for concentrated loads and distributed compressions for small, medium and large angles are indicated in this study. In particularly, the Saint-Venant's principle applied in circular disks subjected to diametral loadings is examined by comparing the full-field results for the concentrated load and the distributed compression with small angle.

2. Full-field analytical solutions for disks subjected to partially distributed compressions

The equations of equilibrium for two-dimensional problems in the polar coordinate are

$$\frac{\partial \sigma_r}{\partial r}+\frac{\sigma_r-\sigma_\theta}{r}+\frac{1}{r}\frac{\partial \tau_{r\theta}}{\partial \theta}=0, \tag{1}$$

$$\frac{1}{r}\frac{\partial \sigma_\theta}{\partial \theta}+\frac{\partial \tau_{r\theta}}{\partial r}+\frac{2\tau_{r\theta}}{r}=0. \tag{2}$$

In the case of plane stress condition, the stress–strain relations for isotropic material are

$$\varepsilon_r=\frac{1}{E}(\sigma_r-v\sigma_\theta), \tag{3}$$

$$\varepsilon_\theta=\frac{1}{E}(\sigma_\theta-v\sigma_r), \tag{4}$$

$$\gamma_{r\theta}=\frac{1}{G}\tau_{r\theta}, \tag{5}$$

where E is the Young's modulus, G is the shear modulus and v is the Poison's ratio. The strain-displacement relations for small strain in the polar coordinate are

$$\varepsilon_r=\frac{\partial u_r}{\partial r}, \tag{6}$$

$$\varepsilon_\theta=\frac{u_r}{r}+\frac{1}{r}\frac{\partial u_\theta}{\partial \theta}, \tag{7}$$

$$\gamma_{r\theta}=\frac{1}{r}\frac{\partial u_r}{\partial \theta}+\frac{\partial u_\theta}{\partial r}-\frac{u_\theta}{r}. \tag{8}$$

2.1. Full-field stresses in explicit functional forms

As shown in Fig. 1, a circular disk loaded by two diametrically opposing distributed compressions located on the top and bottom of the disk is analyzed in this paper. The boundary conditions of this problem are

$$\sigma_r(R,\theta)=-p \quad |\theta|\leqslant\alpha \quad -\frac{\pi}{2}<\theta<\frac{\pi}{2}, \tag{9}$$

$$\sigma_r(R,\theta)=0 \quad |\theta|>\alpha \quad -\frac{\pi}{2}<\theta<\frac{\pi}{2}, \tag{10}$$

$$\tau_{r\theta}(R,\theta)=0 \quad -\frac{\pi}{2}<\theta<\frac{\pi}{2}. \tag{11}$$

Hondros [21] obtained full-field solutions of stresses in series forms as follows:

$$\sigma_r=-\frac{2p}{\pi}\left\{\alpha+\sum_{n=1}^{n=\infty}\left[1-\left(1-\frac{1}{n}\right)\rho^2\right]\rho^{2n-2}\sin 2n\alpha\cos 2n\theta\right\}, \tag{12}$$

$$\sigma_\theta=-\frac{2p}{\pi}\left\{\alpha-\sum_{n=1}^{n=\infty}\left[1-\left(1+\frac{1}{n}\right)\rho^2\right]\rho^{2n-2}\sin 2n\alpha\cos 2n\theta\right\}, \tag{13}$$

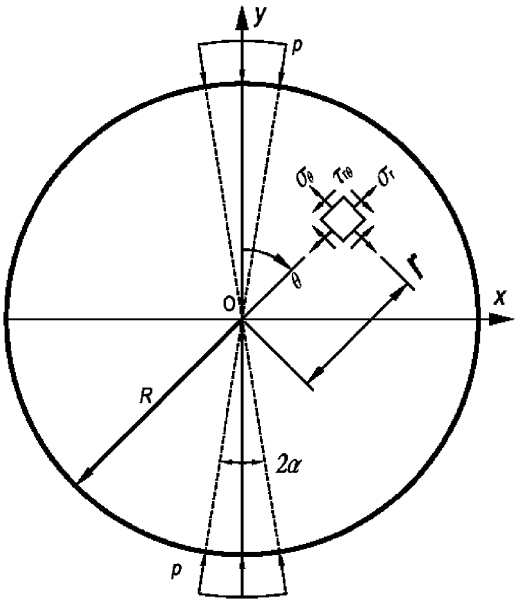

Fig. 1. A circular disk subjected to diametral distributed compression.

$$\tau_{r\theta} = \frac{2p}{\pi}\left\{\sum_{n=1}^{n=\infty}[1-\rho^2]\rho^{2n-2}\sin 2n\alpha \sin 2n\theta\right\}, \tag{14}$$

where σ_r is the normal stress along r-coordinate, σ_θ is the normal stress along θ-coordinate, $\tau_{r\theta}$ is the shear stress with respect to $r-\theta$, p is the applied uniformly distributed traction to be expressed as pressure, 2α is the angle at the origin subtended by the loaded section of the rim, R is the radius of disk, and the ρ is equal to r/R.

Hung and Ma [22] derived the analytical full-field stress distributions in explicit simple functional forms as

$$\sigma_r(\rho,\theta) = -\frac{p}{\pi}\{A_1 + A_2 + B_1 + B_2 + \Phi\} \quad 0 \leqslant \theta \leqslant \frac{\pi}{2}, \tag{15}$$

$$\sigma_\theta(\rho,\theta) = -\frac{p}{\pi}\{-A_1 - A_2 + B_1 + B_2 + \Phi\} \quad 0 \leqslant \theta \leqslant \frac{\pi}{2}, \tag{16}$$

$$\tau_{r\theta}(\rho,\theta) = \frac{p}{\pi}\{C_1 - C_2\} \quad 0 \leqslant \theta \leqslant \frac{\pi}{2}, \tag{17}$$

where

$$A_1 = \frac{(1-\rho^2)\sin 2(\alpha+\theta)}{\rho^4 + 1 - 2\rho^2\cos 2(\alpha+\theta)},$$

$$A_2 = \frac{(1-\rho^2)\sin 2(\alpha-\theta)}{\rho^4 + 1 - 2\rho^2\cos 2(\alpha-\theta)},$$

$$B_1 = \tan^{-1}\left[\frac{1+\rho^2}{1-\rho^2}\tan(\alpha+\theta)\right],$$

$$B_2 = \tan^{-1}\left[\frac{1+\rho^2}{1-\rho^2}\tan(\alpha-\theta)\right],$$

$$C_1 = \frac{(1-\rho^2)[-\rho^2 + \cos 2(\alpha-\theta)]}{\rho^4 + 1 - 2\rho^2\cos 2(\alpha-\theta)},$$

$$C_2 = \frac{(1-\rho^2)[-\rho^2 + \cos 2(\alpha+\theta)]}{\rho^4 + 1 - 2\rho^2\cos 2(\alpha+\theta)},$$

$$\Phi = \begin{cases} 0 & \text{for} \quad 0 \leqslant \theta \leqslant \dfrac{\pi}{2} - \alpha \\ \pi & \text{for} \quad \dfrac{\pi}{2} - \alpha \leqslant \theta \leqslant \dfrac{\pi}{2}. \end{cases}$$

For the two-dimensional problem considered in this paper, we have the condition $\sigma_z = \tau_{zr} = \tau_{z\theta} = 0$ and a state of plane stress exists. The two in-plane principal stresses can be expressed in simple explicit forms

$$\begin{aligned} \sigma_1, \sigma_2 = & -\frac{p}{\pi}\left\{\tan^{-1}\left[\frac{1+\rho^2}{1-\rho^2}\tan(\alpha+\theta)\right] + \tan^{-1}\left[\frac{1+\rho^2}{1-\rho^2}\tan(\alpha-\theta)\right] + \Phi\right\} \\ & \pm \frac{2p}{\pi}(1-\rho^2)\sin 2\alpha \frac{1}{\sqrt{\rho^4 - 2\rho^2\cos 2(\alpha+\theta)+1}\sqrt{\rho^4 - 2\rho^2\cos 2(\alpha-\theta)+1}}. \end{aligned} \tag{18}$$

The maximum shear stress can be worked out easily from Eq. (18). The angle θ_P between x-axis and the principal stress orientation is

$$\theta_p = \frac{1}{2}\tan^{-1}\left[\frac{2\rho^2\cos 2\alpha \sin 2\theta - \rho^4 \sin 4\theta}{1 - 2\rho^2\cos 2\alpha \cos 2\theta + \rho^4 \cos 4\theta}\right]. \tag{19}$$

For the special case of $\alpha = 0$, the problem reduce to a disk subjected to concentrated forces acting along the diameter, the solutions of stresses can be simplified as follows:

$$\sigma_r|_{\alpha\to 0} = \frac{P}{\pi R t}\left\{\frac{(1-\rho^2)^2(\rho^4 + 2\rho^2 - 1 - 2\cos 2\theta)}{(\rho^4 + 1 - 2\rho^2\cos 2\theta)^2}\right\}, \tag{20}$$

$$\sigma_\theta|_{\alpha\to 0} = \frac{P}{\pi R t}\left\{\frac{\rho^8 + 4\rho^4 - 4\rho^2 - 1 + 2(-2\rho^6 + \rho^4 + 1)\cos 2\theta}{(\rho^4 + 1 - 2\rho^2\cos 2\theta)^2}\right\}, \tag{21}$$

$$\tau_{r\theta}|_{\alpha\to 0} = \frac{P}{\pi R t}\left\{\frac{2(1-\rho^4)(1-\rho^2)\sin 2\theta}{(\rho^4 + 1 - 2\rho^2\cos 2\theta)^2}\right\}, \tag{22}$$

where t is the thickness of the disk and P is the magnitude of the applied concentrated force. The solutions expressed in Eqs. (20–22) are the same as those presented by Sokolnikoff [12] with only a negative sign appearing at $\tau_{r\theta}$ to represent the different definition of the orientation of θ.

2.2. Analytical full-field solutions of strain and displacement

For long cylinders (plane strain case) and thin disks (plane stress case), the stress expression given remains unchanged. However, the stress–strain relationships are different. Recalling Eqs. (15–17), the solutions of strain distribution for the plane stress condition can be obtained from the Hooke's Law as follows:

$$\varepsilon_r(\rho,\theta) = \frac{1}{E}(\sigma_r - \nu\sigma_\theta) = -\frac{p}{E\pi}\{(1+\nu)(A_1 + A_2) + (1-\nu)(B_1 + B_2 + \Phi)\} = \frac{\partial u_r}{\partial r}, \tag{23}$$

$$\varepsilon_\theta(\rho,\theta) = \frac{1}{E}(\sigma_\theta - \nu\sigma_r) = -\frac{p}{E\pi}\{-(1+\nu)(A_1 + A_2) + (1-\nu)(B_1 + B_2 + \Phi)\} = \frac{u_r}{r} + \frac{1}{r}\frac{\partial u_\theta}{\partial \theta}, \tag{24}$$

$$\gamma_{r\theta}(\rho,\theta) = \frac{\tau_{r\theta}}{G} = \frac{p}{\pi G}\{C_1 - C_2\}. \tag{25}$$

The displacement u_r can be obtained from Eq. (23) and then u_θ can be constructed using Eq. (24). The full-field solution of u_r is derived first. Integrating Eq. (23) with ρ to obtain

$$u_r = \int \varepsilon_r \, \mathrm{d}r = -\frac{pR}{E\pi}\left\{(1+\nu)\int (A_1 + A_2)\,\mathrm{d}\rho + (1-\nu)\int (B_1 + B_2 + \Phi)\,\mathrm{d}\rho\right\}. \tag{26}$$

The detail integration of Eq. (26) is shown in Appendix A. The full-field solution of displacement u_r is expressed explicitly with a functional form as

$$u_r(\rho,\theta)=-\frac{pR}{E\pi}\left\{\begin{array}{l}\rho\tan^{-1}\left(\frac{1+\rho^2}{1-\rho^2}\tan(\alpha+\theta)\right)+\rho\tan^{-1}\left(\frac{1+\rho^2}{1-\rho^2}\tan(\alpha-\theta)\right)+\rho\Phi\\ +\sin(\alpha+\theta)\ln\left|\frac{1+\rho^2+2\rho\cos(\alpha+\theta)}{1+\rho^2-2\rho\cos(\alpha+\theta)}\right|+\sin(\alpha-\theta)\ln\left|\frac{1+\rho^2+2\rho\cos(\alpha-\theta)}{1+\rho^2-2\rho\cos(\alpha-\theta)}\right|\\ -\cos(\alpha+\theta)\left(\tan^{-1}\frac{\rho\sin(\alpha+\theta)}{1+\rho\cos(\alpha+\theta)}+\tan^{-1}\frac{\rho\sin(\alpha+\theta)}{1-\rho\cos(\alpha+\theta)}\right)-\cos(\alpha-\theta)\left(\tan^{-1}\frac{\rho\sin(\alpha-\theta)}{1+\rho\cos(\alpha-\theta)}+\tan^{-1}\frac{\rho\sin(\alpha-\theta)}{1-\rho\cos(\alpha-\theta)}\right)\\ +v\left[\begin{array}{l}-\rho\tan^{-1}\left(\frac{1+\rho^2}{1-\rho^2}\tan(\alpha+\theta)\right)-\rho\tan^{-1}\left(\frac{1+\rho^2}{1-\rho^2}\tan(\alpha-\theta)\right)-\rho\Phi\\ +\cos(\alpha+\theta)\left(\tan^{-1}\frac{\rho\sin(\alpha+\theta)}{1+\rho\cos(\alpha+\theta)}+\tan^{-1}\frac{\rho\sin(\alpha+\theta)}{1-\rho\cos(\alpha+\theta)}\right)+\cos(\alpha-\theta)\left(\tan^{-1}\frac{\rho\sin(\alpha-\theta)}{1+\rho\cos(\alpha-\theta)}+\tan^{-1}\frac{\rho\sin(\alpha-\theta)}{1-\rho\cos(\alpha-\theta)}\right)\end{array}\right]\end{array}\right\}. \tag{27}$$

Since the displacement u_r is known, the displacement u_θ can be obtained from Eq. (24) as

$$\frac{\partial u_\theta}{\partial\theta}=-\frac{pr}{E\pi}\{-(1+v)(A_1+A_2)+(1-v)(B_1+B_2+\Phi)\}-u_r. \tag{28}$$

As indicated in Eq. (27) that the solution of u_r is a complicated function of θ. Hence, before doing the integration of Eq. (28) with θ, a derivation is made to simplify the expression of Eq. (28) and the result is

$$u_\theta(\rho,\theta)=-\frac{pR}{E\pi}\int\left\{\begin{array}{l}-\rho(1+v)(A_1+A_2)-\left[\begin{array}{l}\sin(\alpha+\theta)\ln\left|\frac{1+\rho^2+2\rho\cos(\alpha+\theta)}{1+\rho^2-2\rho\cos(\alpha+\theta)}\right|\\ +\sin(\alpha-\theta)\ln\left|\frac{1+\rho^2+2\rho\cos(\alpha-\theta)}{1+\rho^2-2\rho\cos(\alpha-\theta)}\right|\end{array}\right]\\ +(1-v)\left[\begin{array}{l}\cos(\alpha+\theta)\left(\tan^{-1}\frac{\rho\sin(\alpha+\theta)}{1+\rho\cos(\alpha+\theta)}+\tan^{-1}\frac{\rho\sin(\alpha+\theta)}{1-\rho\cos(\alpha+\theta)}\right)\\ +\cos(\alpha-\theta)\left(\tan^{-1}\frac{\rho\sin(\alpha-\theta)}{1+\rho\cos(\alpha-\theta)}+\tan^{-1}\frac{\rho\sin(\alpha-\theta)}{1-\rho\cos(\alpha-\theta)}\right)\end{array}\right]\end{array}\right\}\mathrm{d}\theta. \tag{29}$$

It is worthy to note that all the integrations in Eq. (29) can be worked out as simple expressions that are indicated in Appendix B. If we set constrains of displacements $u_r=0$ at $r=0$ and $u_\theta=0$ along $\theta=0$, due to the symmetry of the problem, then the integrating constants are all zero. The complete full-field solution for displacement u_θ can be expressed as the following functional form

$$u_\theta(\rho,\theta)=-\frac{pR}{E\pi}\left\{\begin{array}{l}\sin(\alpha+\theta)\left(\tan^{-1}\frac{\rho\sin(\alpha+\theta)}{1+\rho\cos(\alpha+\theta)}+\tan^{-1}\frac{\rho\sin(\alpha+\theta)}{1-\rho\cos(\alpha+\theta)}\right)-\sin(\alpha-\theta)\left(\tan^{-1}\frac{\rho\sin(\alpha-\theta)}{1+\rho\cos(\alpha-\theta)}+\tan^{-1}\frac{\rho\sin(\alpha-\theta)}{1-\rho\cos(\alpha-\theta)}\right)\\ -\left(\frac{1-\rho^2}{2\rho}\right)\ln\left|\frac{(1+\rho^2)^2-4\rho^2\cos^2(\alpha+\theta)}{(1+\rho^2)^2-4\rho^2\cos^2(\alpha-\theta)}\right|\\ +\frac{1+\rho^2+2\rho\cos(\alpha+\theta)}{2\rho}\ln|1+\rho^2+2\rho\cos(\alpha+\theta)|+\frac{1+\rho^2-2\rho\cos(\alpha+\theta)}{2\rho}\ln|1+\rho^2-2\rho\cos(\alpha+\theta)|\\ -\frac{1+\rho^2+2\rho\cos(\alpha-\theta)}{2\rho}\ln|1+\rho^2+2\rho\cos(\alpha-\theta)|-\frac{1+\rho^2-2\rho\cos(\alpha-\theta)}{2\rho}\ln|1+\rho^2-2\rho\cos(\alpha-\theta)|\\ -v\left[\sin(\alpha+\theta)\left(\tan^{-1}\frac{\rho\sin(\alpha+\theta)}{1+\rho\cos(\alpha+\theta)}+\tan^{-1}\frac{\rho\sin(\alpha+\theta)}{1-\rho\cos(\alpha+\theta)}\right)-\sin(\alpha-\theta)\left(\tan^{-1}\frac{\rho\sin(\alpha-\theta)}{1+\rho\cos(\alpha-\theta)}+\tan^{-1}\frac{\rho\sin(\alpha-\theta)}{1-\rho\cos(\alpha-\theta)}\right)\right]\end{array}\right\} \tag{30}$$

The complete in-plane displacement solutions $u_r(\rho,\theta)$ and $u_\theta(\rho,\theta)$ with functional forms are explicitly expressed in Eqs. (27) and (30), respectively. The solutions for displacements can be checked by substituting Eqs. (27) and (30) into the equilibrium equations for plane stress problems in terms of displacement components relative to polar coordinates as follows:

$$\frac{\partial^2 u_r}{\partial r^2}+\frac{1}{r}\frac{\partial u_r}{\partial r}-\frac{1}{r^2}u_r+\frac{1+v}{2}\frac{1}{r}\frac{\partial^2 u_\theta}{\partial r\,\partial\theta}-\frac{3-v}{2}\frac{1}{r^2}\frac{\partial u_\theta}{\partial\theta}+\frac{1-v}{2}\frac{1}{r^2}\frac{\partial^2 u_r}{\partial\theta^2}=0, \tag{31}$$

$$\frac{1+v}{2}\frac{1}{r}\frac{\partial^2 u_r}{\partial r\partial\theta}+\frac{3-v}{2}\frac{1}{r^2}\frac{\partial u_r}{\partial\theta}+\frac{1-v}{2}\frac{\partial^2 u_\theta}{\partial r^2}+\frac{1-v}{2}\frac{1}{r}\frac{\partial u_\theta}{\partial r}-\frac{1-v}{2}\frac{1}{r^2}u_\theta+\frac{1}{r^2}\frac{\partial^2 u_\theta}{\partial\theta^2}=0. \tag{32}$$

We have checked the results and solutions in Eqs. (27) and (30) satisfy Eqs. (31) and (32) completely.

For the special case of applying concentrated forces, the solutions of displacements are reduced to

$$u_r|_{\alpha\to 0}=-\frac{2P}{E\pi t}\left\{\begin{array}{l}\left[\begin{array}{l}-\dfrac{\rho\left[2+\rho^2+\rho^4-(1+3\rho^2)\cos 2\theta\right]}{1+\rho^4-2\rho^2\cos 2\theta}\\ +\sin\theta\left(\tan^{-1}\dfrac{\rho\sin\theta}{1+\rho\cos\theta}+\tan^{-1}\dfrac{\rho\sin\theta}{1-\rho\cos\theta}\right)+\cos\theta\ln\left|\dfrac{1+\rho^2+2\rho\cos\theta}{1+\rho^2-2\rho\cos\theta}\right|\end{array}\right]\\ +v\left[-\dfrac{\rho(1-\rho^2)(\rho^2-\cos 2\theta)}{1+\rho^4-2\rho^2\cos 2\theta}-\sin\theta\left(\tan^{-1}\dfrac{\rho\sin\theta}{1+\rho\cos\theta}+\tan^{-1}\dfrac{\rho\sin\theta}{1-\rho\cos\theta}\right)\right]\end{array}\right\}, \tag{33}$$

$$u_\theta|_{\alpha\to 0}=-\frac{2P}{E\pi t}\left\{\begin{array}{l}\left[\begin{array}{l}\cos\theta\left(\tan^{-1}\dfrac{\rho\sin\theta}{1+\rho\cos\theta}+\tan^{-1}\dfrac{\rho\sin\theta}{1-\rho\cos\theta}\right)\\ -\sin\theta\left(\dfrac{2\rho(1-\rho^2)\cos\theta}{1+\rho^4-2\rho^2\cos 2\theta}+\ln\left|\dfrac{1+\rho^2+2\rho\cos\theta}{1+\rho^2-2\rho\cos\theta}\right|\right)\end{array}\right]\\ -v\cos\theta\left[\dfrac{2\rho(1-\rho^2)\sin\theta}{1+\rho^4-2\rho^2\cos 2\theta}\right.\\ \left.+\tan^{-1}\dfrac{\rho\sin\theta}{1+\rho\cos\theta}+\tan^{-1}\dfrac{\rho\sin\theta}{1-\rho\cos\theta}\right]\end{array}\right\}. \tag{34}$$

However, for $\alpha=\pi/2$ all the functions in Eqs. (27) and (30) will be cancelled except $\Phi=\pi$, the complicate solutions will reduce to the well-know results of uniform radial tractions as follows:

$$u_r=-\frac{pR}{E\pi}\{\rho\pi-v\rho\pi\}=-\frac{(1-v)}{E}pr,\ u_\theta=0. \tag{35}$$

For the plane stress case, the normal strain ε_z can be easily drived from the two in-plane normal stresses as

$$\begin{aligned}\varepsilon_z&=\frac{\partial u_z}{\partial z}=-v(\varepsilon_r+\varepsilon_\theta)=-\frac{v(1-v)}{E\pi}(\sigma_r+\sigma_\theta)\\ &=\frac{2pv(1-v)}{E\pi}\left\{\tan^{-1}\left[\frac{1+\rho^2}{1-\rho^2}\tan(\alpha+\theta)\right]\right.\\ &\quad\left.+\tan^{-1}\left[\frac{1+\rho^2}{1-\rho^2}\tan(\alpha-\theta)\right]+\Phi\right\}.\end{aligned} \tag{36}$$

The displacement u_z along the thickness direction is obtained in a simple expression as follows:

$$u_z=\int\varepsilon_z\,\mathrm{d}z=\frac{2pv(1-v)}{E\pi}\left\{\tan^{-1}\left[\frac{1+\rho^2}{1-\rho^2}\tan(\alpha+\theta)\right]+\tan^{-1}\left[\frac{1+\rho^2}{1-\rho^2}\tan(\alpha-\theta)\right]+\Phi\right\}z. \tag{37}$$

We can see that the solution of displacement u_z along the thickness direction is much simpler than that of the two in-plane displacements u_r and u_θ. The two in-plane displacements in the Cartesian (x-y) coordinate can be related to the displacements in the polar (r-θ) coordinate as

$$u_x=u_r\sin\theta+u_\theta\cos\theta,\ u_y=u_r\cos\theta-u_\theta\sin\theta,$$

$$\rho=\frac{1}{R}\sqrt{x^2+y^2},\ \theta=\tan^{-1}\frac{x}{y}. \tag{38}$$

It is noted that full-field analytic solutions of strain and displacement for the plane strain condition can be obtained easily from similar derivations.

3. Normal strains and displacements along x- and y-axis

The normal strains and displacements along $x(\theta=\pi/2)$ and $y(\theta=0)$ axis are the two most interesting results for engineering applications and experimental measurements. The solutions along these two lines can be simplified from the results presented in the previous section. It is noted from Eq. (25) that the shear strain along these two lines is zero.

3.1. The normal strains

For $\theta = 0$, we have the normal strains $\varepsilon_r = \varepsilon_y$ and $\varepsilon_\theta = \varepsilon_x$, and the solutions for partially distributed compressions can be reduced from Eqs. (23) and (24) as follows:

$$\varepsilon_r(\rho,0) = \varepsilon_y(\rho,0) = -\frac{2p}{E\pi}\left\{(1+v)\frac{(1-\rho^2)\sin 2\alpha}{\rho^4+1-2\rho^2\cos 2\alpha}+(1-v)\tan^{-1}\left[\frac{1+\rho^2}{1-\rho^2}\right]\tan\alpha\right\}, \tag{39}$$

$$\varepsilon_\theta(\rho,0) = \varepsilon_x(\rho,0) = -\frac{2p}{E\pi}\left\{-(1+v)\frac{(1-\rho^2)\sin 2\alpha}{\rho^4+1-2\rho^2\cos 2\alpha}+(1-v)\tan^{-1}\left[\frac{1+\rho^2}{1-\rho^2}\tan\alpha\right]\right\}. \tag{40}$$

It is interesting to discuss the results at the center ($\rho = 0$) and the boundary ($\rho = 1$) of the disk. The results are reduced from Eqs. (39) and (40) as

$$\varepsilon_r(0,0) = \varepsilon_y(0,0) = -\frac{2p}{E\pi}\{(1+v)\sin 2\alpha + (1-v)\alpha\}, \tag{41}$$

$$\varepsilon_\theta(0,0) = \varepsilon_x(0,0) = -\frac{2p}{E\pi}\{-(1+v)\sin 2\alpha + (1-v)\alpha\}, \tag{42}$$

at the center of the disk and

$$\varepsilon_r(1,0) = \varepsilon_y(1,0) = \varepsilon_\theta(1,0) = \varepsilon_x(1,0) = -\frac{p}{E}(1-v) \tag{43}$$

at the boundary. We can see that the normal strains at the center of the disk are strongly dependent on the distributed angle α. As indicated in Eqs. (41) and (42) that the normal strain at the origin contain functions of $\sin 2\alpha$ and α. Hence, for small value of α, the normal strains are also small and can be further simplified as

$$\varepsilon_r(0,0)_{\alpha\to 0} = \varepsilon_y(0,0)_{\alpha\to 0} = -\frac{2p\alpha}{E\pi}(3+v), \tag{44}$$

$$\varepsilon_\theta(0,0)_{\alpha\to 0} = \varepsilon_x(0,0)_{\alpha\to 0} = \frac{2p\alpha}{E\pi}(1+3v). \tag{45}$$

As shown in Eq. (41) that the normal strain $\varepsilon_r(0,0)$ is always a compressive strain. However, the normal strain $\varepsilon_\theta(0,0)$ is a tensile strain for small and medium value of α, is zero for the condition $(1+v)\sin 2\alpha = (1-v)\alpha$, and is a compressive strain for large value of α. For $v = 0.27$, $\varepsilon_\theta(0,0)$ is zero for $\alpha = 68.35^\circ$. The normal strain $\varepsilon_\theta(0,0)$ at the origin is a tensile strain for $\alpha < 68.35^\circ$ and is a compressive strain for $\alpha > 68.35^\circ$. The maximum tensile strain for $\varepsilon_\theta(0,0)$ is occurred at

$$\alpha = \frac{1}{2}\cos^{-1}\left[\frac{1-v}{2(1+v)}\right], \tag{46}$$

with the magnitude

$$\varepsilon_\theta(0,0) = \varepsilon_x(0,0) = -\frac{2p}{E\pi}\left\{-(1+v)\sqrt{1-\left[\frac{1-v}{2(1+v)}\right]^2}+\frac{1-v}{2}\cos^{-1}\left[\frac{1-v}{2(1+v)}\right]\right\}. \tag{47}$$

The normal strain $\varepsilon_r(0,0)$ has the maximum compressive strain at

$$\alpha = \frac{\pi}{2} - \frac{1}{2}\cos^{-1}\left[\frac{1-v}{2(1+v)}\right], \tag{48}$$

with the magnitude

$$\varepsilon_r(0,0) = \varepsilon_x(0,0) = -\frac{2p}{E\pi}\left\{(1+v)\sqrt{1-\left[\frac{1-v}{2(1+v)}\right]^2}+\frac{1-v}{2}\left[\pi-\cos^{-1}\left(\frac{1-v}{2(1+v)}\right)\right]\right\}. \tag{49}$$

The normal strains at the boundary presented in Eq. (43) are independent on the distributed angle α and have the same solutions as that of applying uniform compression (i.e., $\alpha = \pi/2$).

For the case of applying concentrated loads, we have very simple expressions of the solutions for $\theta = 0$ as follows:

$$\varepsilon_r(\rho,0) = \varepsilon_y(\rho,0) = -\frac{P}{E\pi Rt}\left\{\frac{3+\rho^2}{1-\rho^2}+v\right\}, \tag{50}$$

$$\varepsilon_\theta(\rho,0)=\varepsilon_x(\rho,0)=\frac{P}{E\pi Rt}\left\{1+v\frac{3+\rho^2}{1-\rho^2}\right\}. \tag{51}$$

It is indicated in Eqs. (50) and (51) that the normal strains are singular at the boundary ($\rho=1$) by applying concentrated loads. The normal strains at the center of the disk are

$$\varepsilon_r(0,0)=\varepsilon_y(0,0)=-\frac{P}{E\pi Rt}\{3+v\}, \tag{52}$$

$$\varepsilon_\theta(0,0)=\varepsilon_x(0,0)=\frac{P}{E\pi Rt}\{1+3v\}. \tag{53}$$

It is interesting to note that Eqs. (52) and (53) have the same forms if compared with the results for partially distributed compressions with small α as presented in Eqs. (44) and (45) by substituting $P=2p\alpha Rt$. The normal strains along the x-axis are presented in Appendix C.

3.2. The displacements

For $\theta=0$, the displacements for partially distributed compressions are obtained from Eqs. (27) and (30)

$$u_r(\rho,0)=u_y(\rho,0)=-\frac{2pR}{E\pi}\left\{(1-v)\rho\tan^{-1}\left(\frac{1+\rho^2}{1-\rho^2}\tan\alpha\right)+\sin\alpha\ln\left|\frac{1+\rho^2+2\rho\cos\alpha}{1+\rho^2-2\rho\cos\alpha}\right|\right.$$
$$\left.-(1-v)\cos\alpha\left[\tan^{-1}\left(\frac{\rho\sin\alpha}{1+\rho\cos\alpha}\right)+\tan^{-1}\left(\frac{\rho\sin\alpha}{1-\rho\cos\alpha}\right)\right]\right\}, \tag{54}$$

$$u_\theta(\rho,0)=u_x(\rho,0)=0 \tag{55}$$

For applying concentrated loads, the solutions are reduced from Eqs. (33) and (34), and the results are

$$u_r(\rho,0)=u_y(\rho,0)=-\frac{2P}{E\pi t}\left\{-(1-v)\rho+2\ln\left|\frac{1+\rho}{1-\rho}\right|\right\}, \tag{56}$$

$$u_\theta(\rho,0)=u_x(\rho,0)=0. \tag{57}$$

For $\theta=\pi/2$, the displacements for partially distributed compressions are

$$u_r(\rho,\pi/2)=u_x(\rho,\pi/2)=-\frac{2pR}{E\pi}\left\{(1-v)\rho\cot^{-1}\left(\frac{1+\rho^2}{1-\rho^2}\cot\alpha\right)+\cos\alpha\ln\left|\frac{1+\rho^2-2\rho\sin\alpha}{1+\rho^2+2\rho\sin\alpha}\right|\right.$$
$$\left.+(1-v)\sin\alpha\left[\tan^{-1}\left(\frac{\rho\cos\alpha}{1+\rho\sin\alpha}\right)+\tan^{-1}\left[\left(\frac{\rho\cos\alpha}{1-\rho\sin\alpha}\right)\right]\right]\right\}, \tag{58}$$

$$u_\theta(\rho,\pi/2)=u_y(\rho,\pi/2)=0. \tag{59}$$

For applying concentrated loads, the results are

$$u_r(\rho,\pi/2)=u_x(\rho,\pi/2)=-\frac{2P}{E\pi t}\left\{-\frac{\rho}{\rho^2+1}[(\rho^2+3)-v(1-\rho^2)]+2(1-v)\tan^{-1}\rho\right\}, \tag{60}$$

$$u_\theta(\rho,\pi/2)=u_y(\rho,\pi/2)=0. \tag{61}$$

4. Numerical analysis

Base on the analytical full-field solutions with explicit functional forms provided in the previous section, a complete numerical calculation and detail discussions of strain and displacement will be given in this section. The numerical calculations for full-field distributions of strains and displacements are easy to perform without introducing any numerical errors. We use $v=0.27$ for all numerical calculations. For contour plots, the solid-line and dashed-line represent positive and negative values, respectively. Four different values of the angle of distributed compressions are used for numerical investigations, there are $\alpha=0^\circ$ (concentrated force), $\alpha=4.5^\circ$ (small angle), $\alpha=30^\circ$ (medium angle), and $\alpha=60^\circ$ (large angle).

For $\alpha=0^\circ$, the nondimensional normal strain $\varepsilon_r/(P/ERt)$ for applying concentrated loads is shown in Fig. 2(a), and full-field distributions of $\varepsilon_r/(p/E)$ with $\alpha=4.5^\circ$, 30°, 60° are shown in Figs. 2(b)–(d). It is shown in Figs. 2(a) and (b) for the

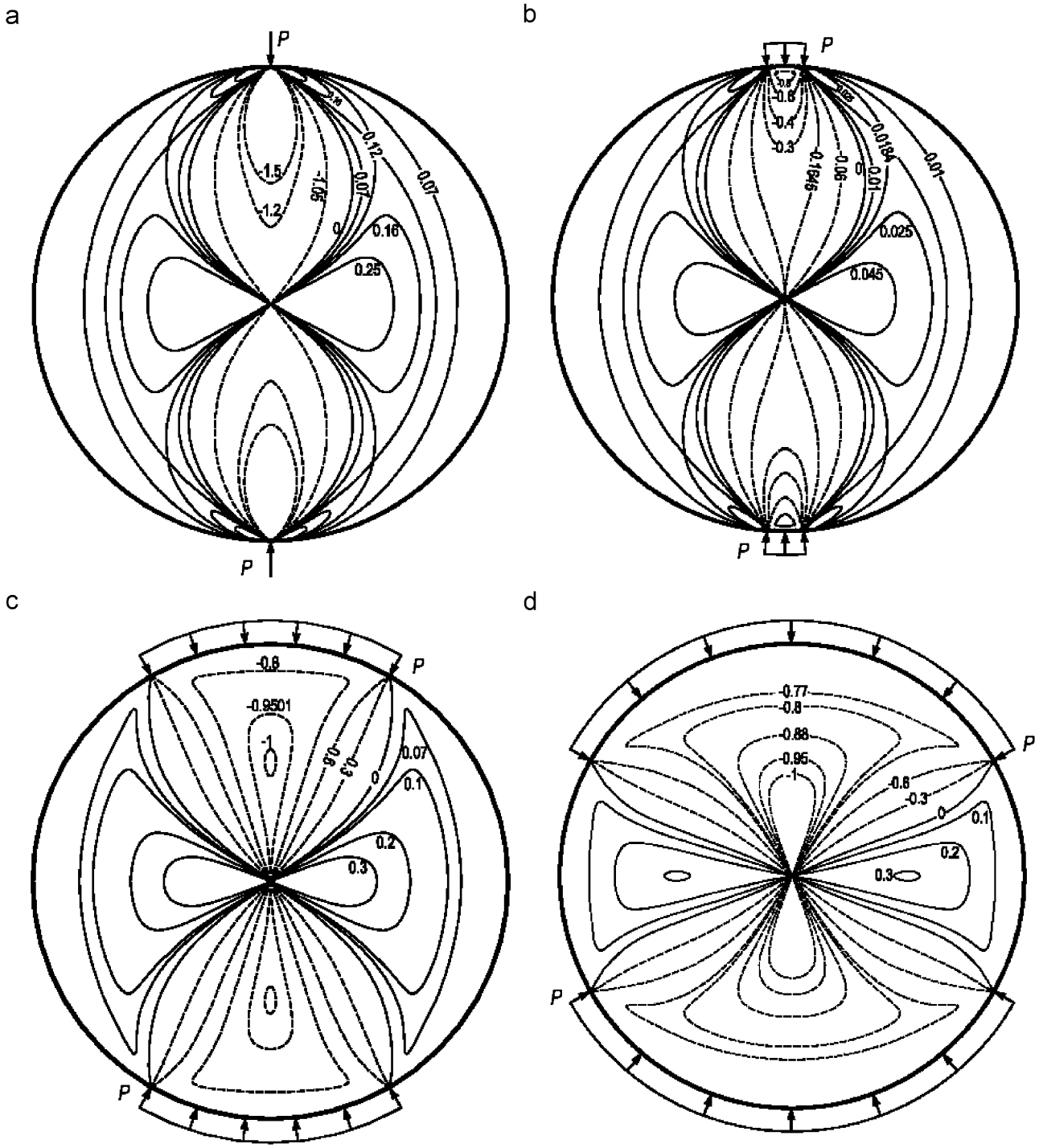

Fig. 2. (a) The normal strain $\varepsilon_r/(P/ERt)$ contours for $\alpha = 0^\circ$; (b) the normal strain $\varepsilon_r/(p/E)$ contours for $\alpha = 4.5^\circ$; (c) the normal strain $\varepsilon_r/(p/E)$ contours for $\alpha = 30^\circ$ and (d) the normal strain $\varepsilon_r/(p/E)$ contours for $\alpha = 60^\circ$.

concentrated load and the distributed compression with small angle that the full-field distributions are similar except in the small area near the boundary where the loading is applied. If we set $P = 2p\alpha Rt$ in Fig. 2(a) and normalize the strain as indicated in Fig. 2(b), then the magnitude of the normal strain in Fig. 2(a) will be nearly the same as that presented in Fig. 2(b) except in the small area near the loading boundary. Figs. 2(a) and (b) show the clear explanation of the Saint-Venant's principle applied in a circular disk. It is indicated in these figures that the compressive strain is confined in the region between the partial distribution of the applied compressive loads and the center of the disk. Local maximum values of compressive strain are developed near the boundary of distributed loads and in the middle area for $\alpha = 4.5^\circ$(Fig. 2(b)) and for $\alpha = 30^\circ$ (Fig. 2(c)), respectively. For large value of α (Fig. 2(d)), we can see that a constant state with the magnitude $\varepsilon_r = -0.73p/E$ will be developed near the distributed compression boundary. Finally, this constant region spread out of the

whole disk for $\alpha = 90^\circ$. It is also indicated in Fig. 2(d) that a local maximum value of tensile strain is developed in the middle of the line $\theta = \pi/2$. The detailed functional forms of $\varepsilon_r(\rho,0)$ ($\varepsilon_r(\rho,\pi/2)$) along the line $\theta = 0$ ($\theta = \pi/2$) are presented in Eq. (39) ((C.1)) for partially distributed compressions and in Eq. (50) ((C.5)) for concentrated loads. The maximum normal strain at the origin for partially distributed compressions $\varepsilon_r(0,0)$ for $v = 0.27$ will occur at $\alpha = 53.35^\circ$ (from Eq. (48)) and the magnitude is $-1.2071p/E$ (from Eq. (49)).

The full-field distribution for applying concentrated load ($\alpha = 0^\circ$) of $\varepsilon_\theta/(P/ERt)$ is presented in Fig. 3(a), and distributions of $\varepsilon_\theta/(p/E)$ with $\alpha = 4.5^\circ$, 30°, 60° are shown in Figs. 3(b)–(d). Base on the Saint-Venant's principle, it is also clearly indicated in Figs. 3(a) and (b) that the contour plots of these two figures is similar except near the boundary region where the loading is applied. We can see that as the value of α increases, the regions of tensile normal strain are confined in

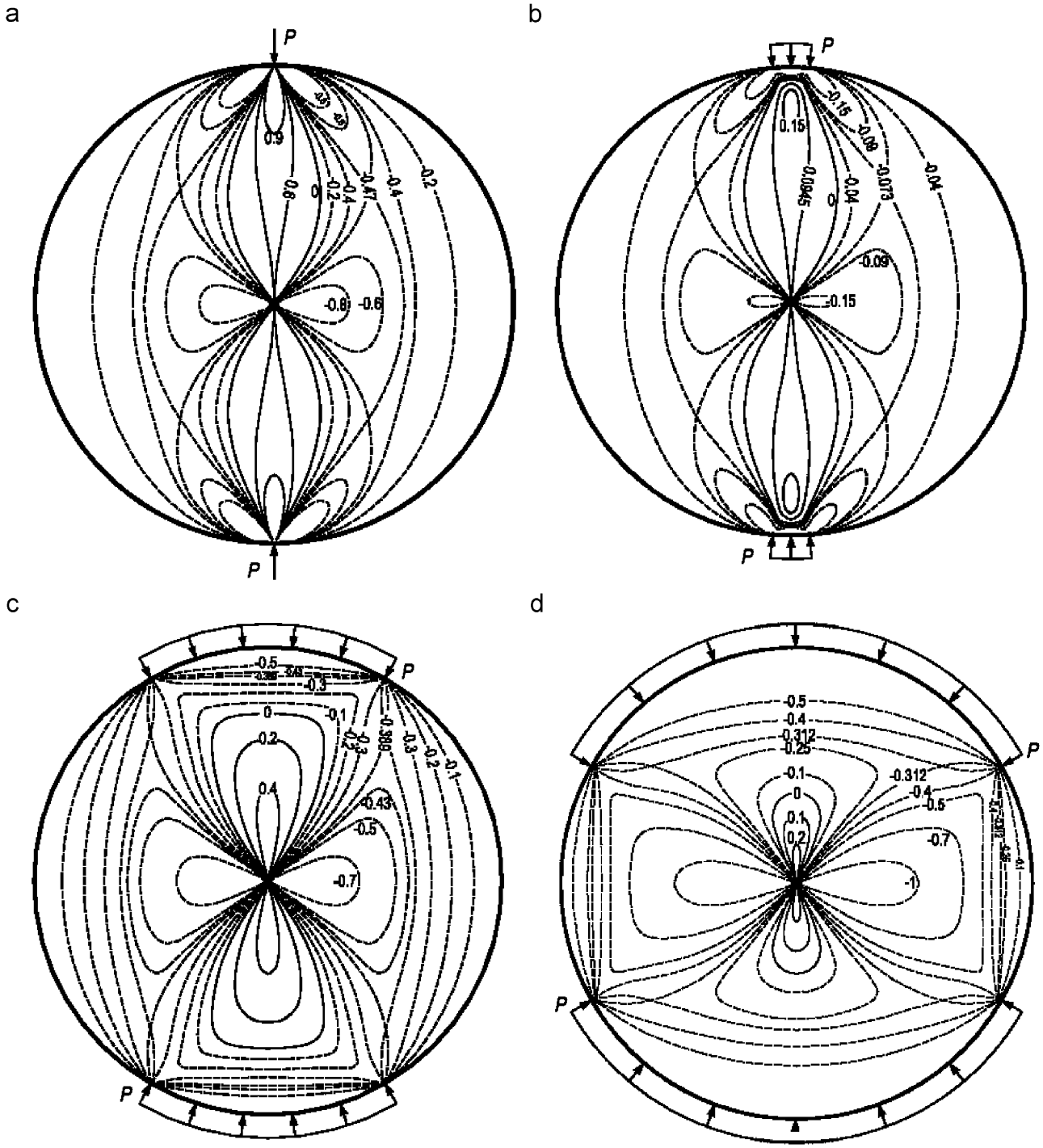

Fig. 3. (a) The normal strain $\varepsilon_\theta/(P/ERt)$ contours for $\alpha = 0^\circ$; (b) the normal strain $\varepsilon_\theta/(p/E)$ contours for $\alpha = 4.5^\circ$; (c) The normal strain $\varepsilon_\theta/(p/E)$ contours for $\alpha = 30^\circ$ and (d) the normal strain $\varepsilon_\theta/(p/E)$ contours for $\alpha = 60^\circ$.

small areas along the vertical direction near the center of the disk and larger values of the compressive strain will develop along the horizontal axis. For $\alpha = 90^\circ$, a constant state with the magnitude $\varepsilon_\theta = -0.73p/E$ will occupy the whole disk. The detailed functional forms of $\varepsilon_\theta(\rho,0)$ ($\varepsilon_\theta(\rho,\pi/2)$) along the line $\theta = 0$ ($\theta = \pi/2$) are indicated in Eq. (40) ((C.2)) for partially distributed compressions and in Eq. (51) ((C.6)) for concentrated load. As indicated in the previous section that the normal $\varepsilon_\theta(0,0)$ is a tensile strain for α is smaller than a critical value which is determined by the condition $(1+\nu)\sin 2\alpha = (1-\nu)\alpha$. The critical angle is $\alpha = 68.35^\circ$ for $\nu = 0.27$. For $\alpha > 68.35^\circ$, the normal strain $\varepsilon_\theta(0,0)$ is a compressive strain. The maximum tensile normal strain $\varepsilon_\theta(0,0)$ for $\nu = 0.27$ will occur at $\alpha = 36.65^\circ$ (from Eq. (46)) and the magnitude is $0.4771p/E$ (from Eq. (47)). The above-mentioned phenomenon is also clearly shown in Figs. 3(b)–(d).

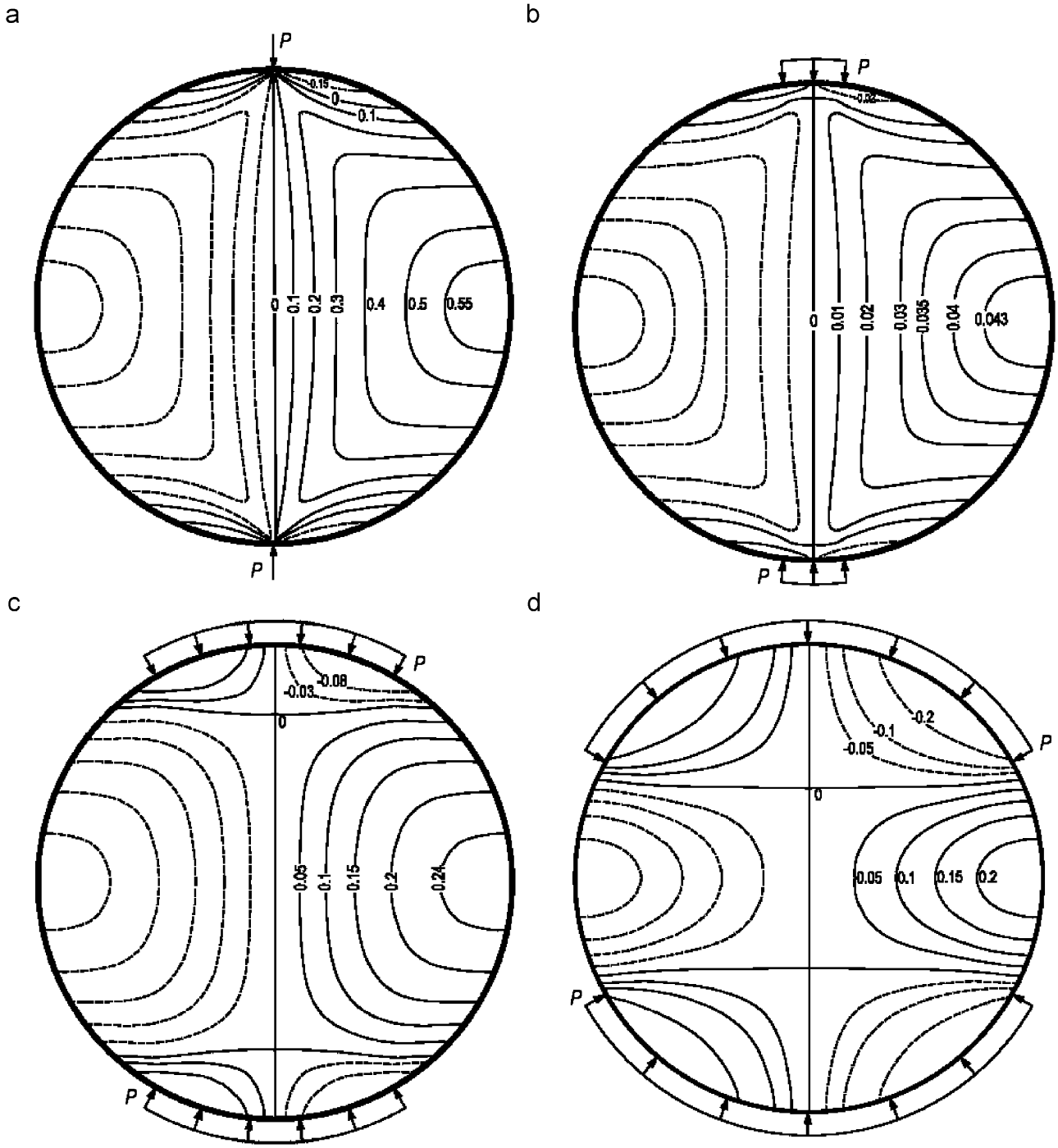

Fig. 4. (a) The displacement $u_x/(P/Et)$ contours for $\alpha = 0^\circ$; (b) the displacement $u_x/(pR/E)$ contours for $\alpha = 4.5^\circ$; (c) The displacement $u_x/(pR/E)$ contours for $\alpha = 30^\circ$ and (d) the displacement $u_x/(pR/E)$ contours for $\alpha = 60^\circ$.

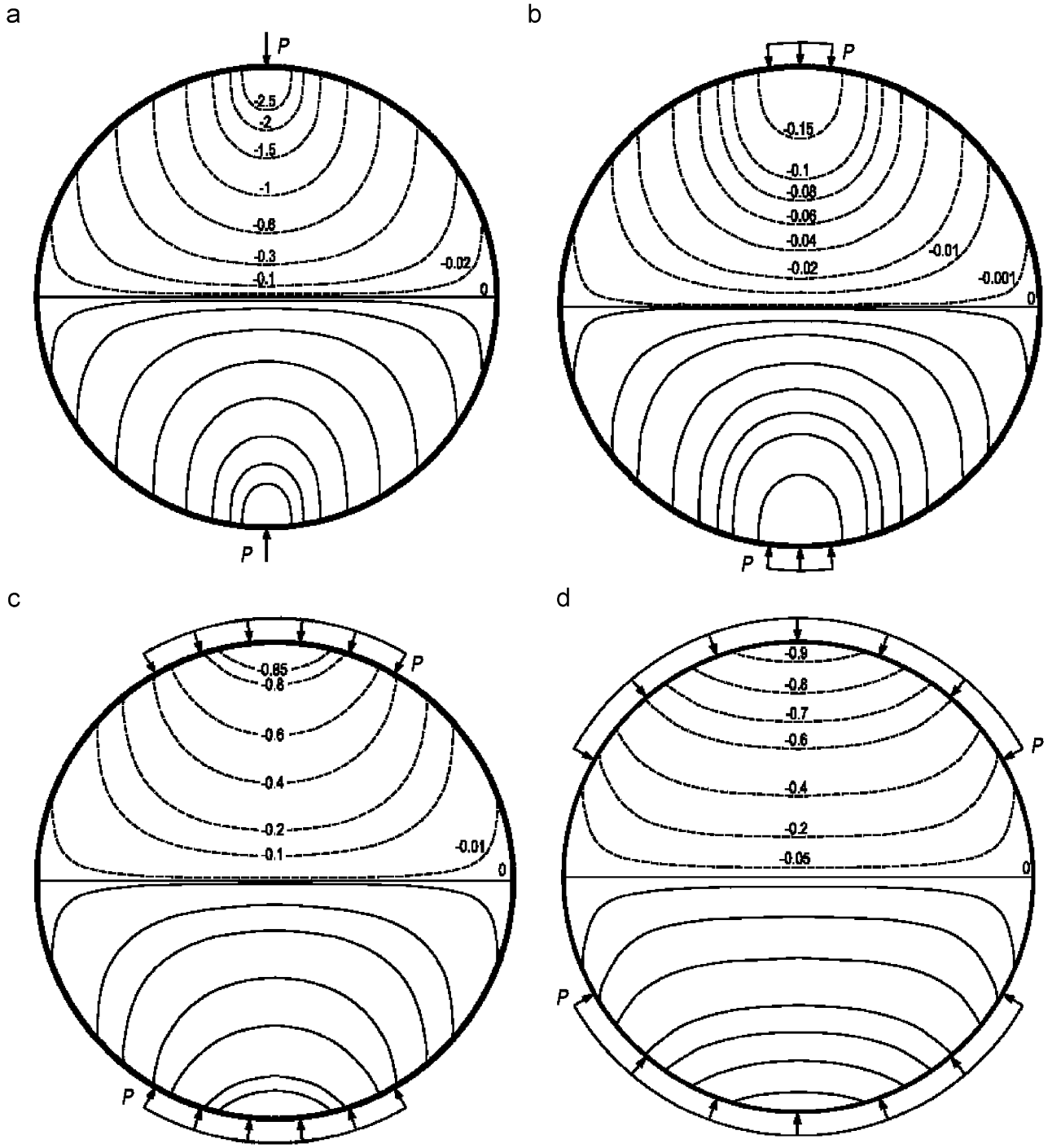

Fig. 5. (a) The displacement $u_y/(P/Et)$ contours for $\alpha = 0°$; (b) the displacement $u_y/(pR/E)$ contours for $\alpha = 4.5°$; (c) The displacement $u_y/(pR/E)$ contours for $\alpha = 30°$ and (d) the displacement $u_y/(pR/E)$ contours for $\alpha = 60°$.

Figs. 4 and 5 are contour plots of displacements in Cartesian coordinate for different loading conditions. Moiré fringe patterns can be interpreted by relating them to in-plane displacement fields. Hence the full-field distributions of displacements u_x and u_y can be used to compare with the experimental results using the Moiré interferometry technique. Fig. 6 shows the experimental results of a series of Moiré and associated photoelastic observations conducted by Durelli (Timoshenko and Goodier [10]) for a thin disk subjected to diametrically loads. The upper-left quadrant in Fig. 6 shows the Moiré contours of horizontal displacement u_x. The lower-left quadrant shows the contours of vertical displacement u_y. It is worthy to note that the experimental results of displacement contours u_x and u_y shown in Fig. 6 excellently agree with the theoretical predictions as indicated in Fig. 4(a) (or Fig. 4(b)) and Fig. 5(a) (or Fig. 5(b)). The lower-right quadrant in Fig. 6 indicates the isochromatics for a disk loaded diametrically. For theoretical analysis, the isochromatic fringe pattern gives

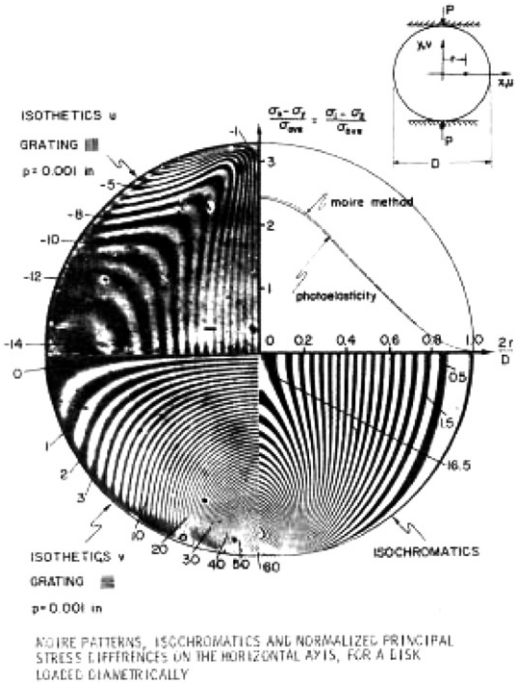

Fig. 6. Experimental results of Moiré and photoelastic by Durelli. (Timoshenko and Goodier [10]).

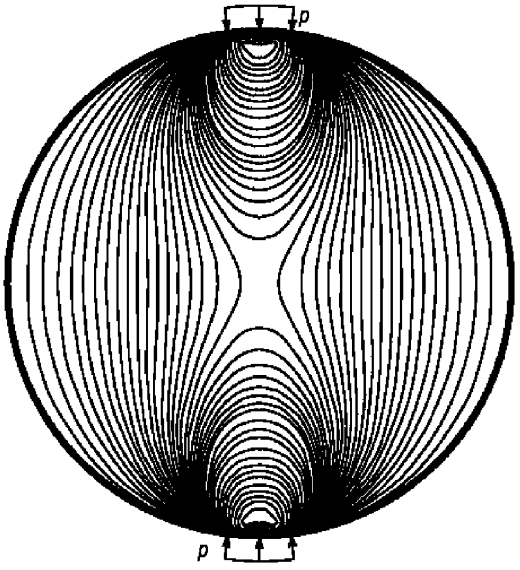

Fig. 7. The Isochromatics for $\alpha = 4.5^{\circ}$ from theoretical prediction.

lines for which the principal stress difference is equal to a constant. Since the solutions of the two principal stresses are given explicitly in Eq. (18), the principal stress difference for the problem of a disk subjected to partially distributed compressions is easily obtained. Fig. 7 shows the theoretical prediction of the isochromatics for $\alpha = 4.5^{\circ}$ and the result matches very well with the experimental measurement presented in Fig. 6. It is clearly shown in Fig. 7 that the maximum value is not on the boundary but produces a local fringe near the boundary. This local maximum is also found in the isochromatics near the boundary presented in Fig. 6. It is noted that for truly concentrated loads, the fringes should originate at the point of the applied concentrated load. From the evidences provided by the experimental observation and the theoretical analysis of displacements and isochromatics, it can be concluded that the actual loading applied at the disk for Fig. 6 is not a truly concentrated load but a partially distributed compression with small angle. Fig. 8 shows the displacement distribution u_z along the thickness direction.

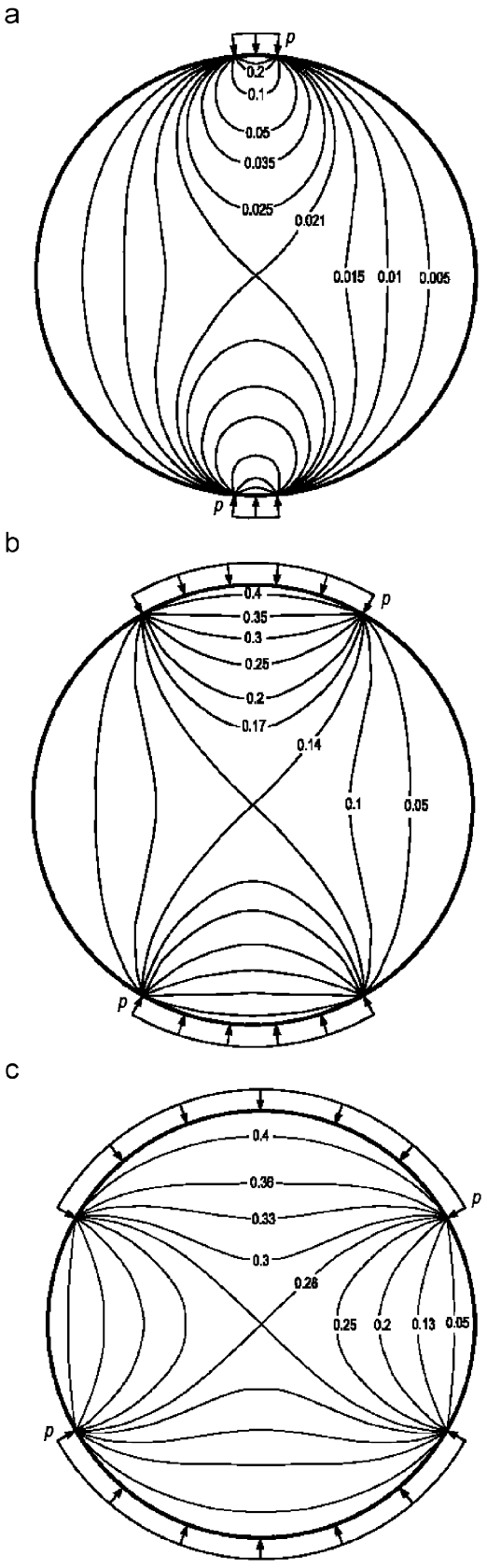

Fig. 8. (a) The displacement $u_z/(pz/E\pi)$ contours for $\alpha = 4.5^\circ$; (b) the displacement $u_z/(pz/E\pi)$ contours for $\alpha = 30^\circ$ and (c) The displacement $u_z/(pz/E\pi)$ contours for $\alpha = 60^\circ$.

5. Conclusions

On developing experimental mechanics, a disk subjected to diametral compressions is an important problem to be quoted to illustrate new theories and experimental techniques. The compression is usually idealized to be a concentrated force of reverse direction because it can be compared with the existed theoretical solution. However, disk in diametral compression on an area is the real situation of experimental condition and engineering application; and there is a lack of theoretical solution expressed in a concise form. This paper provides full-field analytic solutions of strain and displacement for the problem of a disk subjected to diametral compression on a finite area at rim. Furthermore, these solutions are all expressed in simple explicit functional forms that can be easily used as a theoretical reference to compare with experimental results. Full-field distributions of strain and displacement are provided by numerical calculations base on the analytical solutions. Detail discussions of interesting phenomena of strains and displacements for a disk subjected to concentrated loads and distributed compressions for small, medium and large angles are made. The Saint-Venant's principle applied in a circular disk is examined by comparing the full-field contour plots for concentrated loads and distributed compressions with small angle. Experimental measurements of full-field displacement contours and isochromatic fringe patterns are used to compare with the theoretical predictions and good agreements of both results are found.

Acknowledgment

The research support of the National Science Council, Republic of China, through Grant NSC 90-2212-E002-230 at National Taiwan University is gratefully acknowledged.

Appendix A. The detail integration of Eq. (26)

The first integrating term in Eq. (26) is obtained explicitly as

$$\int A_1 \,\mathrm{d}\rho = \sin 2(\alpha+\theta)\int \frac{1-\rho^2}{\rho^4+1-2\rho^2\cos 2(\alpha+\theta)}\,\mathrm{d}\rho = \frac{\sin(\alpha+\theta)}{2}\ln\left|\frac{1+\rho^2+2\rho\cos(\alpha+\theta)}{1+\rho^2-2\rho\cos(\alpha+\theta)}\right|. \tag{A.1}$$

Similarly, the result for second integrating term in Eq. (26) is

$$\int A_2 \,\mathrm{d}\rho = \frac{\sin(\alpha-\theta)}{2}\ln\left|\frac{1+\rho^2+2\rho\cos(\alpha-\theta)}{1+\rho^2-2\rho\cos(\alpha-\theta)}\right|. \tag{A.2}$$

The third integrating term in Eq. (26) can be worked out as

$$\int B_1 \,\mathrm{d}\rho = \int \tan^{-1}\left(\frac{1+\rho^2}{1-\rho^2}\tan(\alpha+\theta)\right)\mathrm{d}\rho = \left\{\begin{array}{l} \rho\tan^{-1}\left(\dfrac{1+\rho^2}{1-\rho^2}\tan(\alpha+\theta)\right)+\dfrac{\sin(\alpha+\theta)}{2}\ln\left|\dfrac{1+\rho^2+2\rho\cos(\alpha+\theta)}{1+\rho^2-2\rho\cos(\alpha+\theta)}\right| \\ -\cos(\alpha+\theta)\left(\tan^{-1}\left(\dfrac{\rho\sin(\alpha+\theta)}{1+\rho\cos(\alpha+\theta)}\right)+\tan^{-1}\left(\dfrac{\rho\sin(\alpha+\theta)}{1-\rho\cos(\alpha-\theta)}\right)\right) \end{array}\right\}. \tag{A.3}$$

Similarly, the result for the fourth term in Eq. (26) is

$$\int B_2 \,\mathrm{d}\rho = \left\{\begin{array}{l} \rho\tan^{-1}\left(\dfrac{1+\rho^2}{1-\rho^2}\tan(\alpha-\theta)\right)+\dfrac{\sin(\alpha-\theta)}{2}\ln\left|\dfrac{1+\rho^2+2\rho\cos(\alpha-\theta)}{1+\rho^2-2\rho\cos(\alpha-\theta)}\right| \\ -\cos(\alpha-\theta)\left(\tan^{-1}\left(\dfrac{\rho\sin(\alpha-\theta)}{1+\rho\cos(\alpha-\theta)}\right)+\tan^{-1}\left(\dfrac{\rho\sin(\alpha-\theta)}{1-\rho\cos(\alpha-\theta)}\right)\right) \end{array}\right\}. \tag{A.4}$$

Appendix B. The detail integration of Eq. (29)

The first two integration terms in Eq. (29) can be worked out as

$$\int (A_1+A_2)\,\mathrm{d}\theta = \frac{1-\rho^2}{4\rho^2}\ln\left|\frac{(1+\rho^2)^2-4\rho^2\cos^2(\alpha+\theta)}{(1+\rho^2)^2-4\rho^2\cos^2(\alpha-\theta)}\right|, \tag{B.1}$$

and

$$\int \left[\sin(\alpha+\theta)\ln\left|\frac{1+\rho^2+2\rho\cos(\alpha+\theta)}{1+\rho^2-2\rho\cos(\alpha+\theta)}\right|+\sin(\alpha-\theta)\ln\left|\frac{1+\rho^2+2\rho\cos(\alpha-\theta)}{1+\rho^2-2\rho\cos(\alpha-\theta)}\right|\right]d\theta$$
$$=-\frac{1}{2\rho}\begin{bmatrix}(1+\rho^2+2\rho\cos(\alpha+\theta))\ln|1+\rho^2+2\rho\cos(\alpha+\theta)|\\+(1+\rho^2-2\rho\cos(\alpha+\theta))\ln|1+\rho^2-2\rho\cos(\alpha+\theta)|\\-(1+\rho^2+2\rho\cos(\alpha-\theta))\ln|1+\rho^2+2\rho\cos(\alpha-\theta)|\\-(1+\rho^2-2\rho\cos(\alpha-\theta))\ln|1+\rho^2-2\rho\cos(\alpha-\theta)|\end{bmatrix}, \tag{B.2}$$

$$\int \cos(\alpha+\theta)\left[\tan^{-1}\frac{\rho\sin(\alpha+\theta)}{1+\rho\cos(\alpha+\theta)}+\tan^{-1}\frac{\rho\sin(\alpha+\theta)}{1-\rho\cos(\alpha+\theta)}\right]d\theta$$
$$=\begin{bmatrix}\sin(\alpha+\theta)\left[\tan^{-1}\frac{\rho\sin(\alpha+\theta)}{1+\rho\cos(\alpha+\theta)}+\tan^{-1}\frac{\rho\sin(\alpha+\theta)}{1-\rho\cos(\alpha+\theta)}\right]\\-\frac{1-\rho^2}{4\rho}\ln|(1+\rho^2)^2-4\rho^2\cos^2(\alpha+\theta)|\end{bmatrix}. \tag{B.3}$$

Similarly, we have

$$\int \cos(\alpha-\theta)\left[\tan^{-1}\frac{\rho\sin(\alpha-\theta)}{1+\rho\cos(\alpha-\theta)}+\tan^{-1}\frac{\rho\sin(\alpha-\theta)}{1-\rho\cos(\alpha-\theta)}\right]d\theta$$
$$=\begin{bmatrix}-\sin(\alpha-\theta)\left[\tan^{-1}\frac{\rho\sin(\alpha-\theta)}{1+\rho\cos(\alpha-\theta)}+\tan^{-1}\frac{\rho\sin(\alpha-\theta)}{1-\rho\cos(\alpha-\theta)}\right]\\+\frac{1-\rho^2}{4\rho}\ln|(1+\rho^2)^2-4\rho^2\cos^2(\alpha-\theta)|\end{bmatrix}. \tag{B.4}$$

Appendix C. The normal strains along the *x*-axis

For $\theta=\pi/2$, we have the normal strains $\varepsilon_r=\varepsilon_x$ and $\varepsilon_\theta=\varepsilon_y$. The solutions for partially distributed compressions are

$$\varepsilon_r(\rho,\pi/2)=\varepsilon_x(\rho,\pi/2)=-\frac{2p}{E\pi}\left\{-(1+\nu)\frac{(1-\rho^2)\sin 2\alpha}{\rho^4+1+2\rho^2\cos 2\alpha}+(1-\nu)\cot^{-1}\left[\frac{1+\rho^2}{1-\rho^2}\cot\alpha\right]\right\}, \tag{C.1}$$

$$\varepsilon_\theta(\rho,\pi/2)=\varepsilon_y(\rho,\pi/2)=-\frac{2p}{E\pi}\left\{(1+\nu)\frac{(1-\rho^2)\sin 2\alpha}{\rho^4+1+2\rho^2\cos 2\alpha}+(1-\nu)\cot^{-1}\left[\frac{1+\rho^2}{1-\rho^2}\cot\alpha\right]\right\}. \tag{C.2}$$

The normal strains at the center of the disk are

$$\varepsilon_r(0,\pi/2)=\varepsilon_x(0,\pi/2)=-\frac{2p}{E\pi}\{-(1+\nu)\sin 2\alpha+(1-\nu)\alpha\}, \tag{C.3}$$

$$\varepsilon_\theta(0,\pi/2)=\varepsilon_y(0,\pi/2)=-\frac{2p}{E\pi}\{(1+\nu)\sin 2\alpha+(1-\nu)\alpha\}. \tag{C.4}$$

The normal strains at the boundary $\rho=1$ are zero, i.e. $\varepsilon_r(1,\pi/2)=\varepsilon_x(1,\pi/2)=\varepsilon_\theta(1,\pi/2)=\varepsilon_y(1,\pi/2)=0$, except $\alpha=\pi/2$.

For the case of applying concentrated loads, we have the solutions for $\theta=\pi/2$ as follows:

$$\varepsilon_r(\rho,\pi/2)=\varepsilon_x(\rho,\pi/2)=\frac{P}{E\pi Rt}\left\{\left(\frac{1-\rho^2}{1+\rho^2}\right)^2-\nu\left[\frac{\rho^8+4\rho^6+2\rho^4-4\rho^2-3}{(1+\rho^2)^4}\right]\right\}, \tag{C.5}$$

$$\varepsilon_\theta(\rho,\pi/2)=\varepsilon_y(\rho,\pi/2)=\frac{P}{E\pi Rt}\left\{\left[\frac{\rho^8+4\rho^6+2\rho^4-4\rho^2-3}{(1+\rho^2)^4}\right]-\nu\left(\frac{1-\rho^2}{1+\rho^2}\right)^2\right\}. \tag{C.6}$$

The normal strains at the center of the disk for applying concentrated loads are

$$\varepsilon_r(0,\pi/2) = \varepsilon_x(0,\pi/2) = \frac{P}{E\pi Rt}\{1+3v\}, \tag{C.7}$$

$$\varepsilon_\theta(0,\pi/2) = \varepsilon_y(0,\pi/2) = -\frac{P}{E\pi Rt}\{3+v\}. \tag{C.8}$$

References

[1] Chong KP, Smith JW, Borgman ES. Tensile strengths of Colorado and Utah oil shales. AIAA Journal of Energy 1982;6:81–5.
[2] Carneiro FLLB. A new method to determine the tensile strength of concrete. In: Proceedings of the fifth meeting of the Brazilian association for technical rules; 1943. 126–129.
[3] Akazawa T. Méthode pour léssai de traction de bétons. Journal of the Japanese Civil Engineering Institute 1943, republished in French by bulletin RILEM 1953;16:13–23.
[4] Fairbairn EMR, Ulm FJ. A tribute to Fernando L.L.B. Carneiro (1913–2001) engineer and scientist who invented the Brazilian test. Material and Structure 2002;35:195–6.
[5] Claesson J, Bohloli B. Brazilian test: stress field and tensile strength of anisotropic rocks using an analytical solution. International Journal of Rock Mechanics and Mining Sciences 2002;39:991–1004.
[6] Cauwelaert FV, Eckmann B. Indirect tensile test applied to anisotropic material. Material and Structure 1994;27:54–6.
[7] Sato S, Awaji H, Akuzawa H. Fracture toughness of reactor graphite at high temperature. Carbon 1978;16:95–102.
[8] Awaji H, Sato S. Diametral compressive test method. Journal of Engineering Materials and Technology 1979;101:139–47.
[9] Frocht MM. Photoelasticity II. New York: Wiley; 1948. p. 131–55.
[10] Timoshenko SP, Goodier JN. Theory of elasticity. 3rd ed. Singapore: McGraw-Hill; 1982. p. 166–67.
[11] Muskhelishvili NI. Some basic problems of the mathematical theory of elasticity. The Netherlands: Noordhoff International Publishing; 1975.
[12] Sokolnikoff IS. Mathematical theory of elasticity. Singapore: McGraw-Hill; 1956. p. 283–84.
[13] Pindera JT, Pindera MJ. Isodyne stress analysis. The Netherlands: Kluwer Academic Publishers; 1989.
[14] Fairhurst C. On the validity of the Brazilian test for brittle materials. International Journal of Rock Mechanics and Mining Sciences 1964;1:535–46.
[15] Voloshin AS, Burger CP. Half-fringe photoelasticity: a new approach to whole-field stress analysis. Experimental Mechanics 1983;23:304–13.
[16] Brown GM, Sullivan JL. The computer-aided holophotoelastic method. Experimental Mechanics 1990;30:135–44.
[17] Chen TY, Chen TF. Whole-field digital measurements of isocharmatics and isoclinics in photoelastic coatings. Optics and Lasers Engineering 1999;31:325–38.
[18] Durelli A, Ferrer L. New methods to determine elastic constants. Materials Research and Standards 1963;3:988–91.
[19] Cárdenas-García J. The Moiré circular disk: two inverse problems. Mechanics Research Communications 2001;28:381–8.
[20] Wang Z, Cárdenas-García J, Han B. Inverse method to determine elastic constants using a circular disk and Moiré interferometry. Experimental Mechanics 2005;45:27–34.
[21] Hondros G. The evaluation of Poisson's ratio and the modulus of materials of a low tensile resistance by the Brazilian test. Australia Journal of Applied Science 1959;10:243–68.
[22] Hung KM, Ma CC. Theoretical analysis and digital photoelastic measurement of circular disks subjected to partially distributed compressions. Experimental Mechanics 2003;43:216–24.
[23] Davison T, Wadley HNG, Pindera MJ. Elastic response of a layered cylinder subjected to diametral loading. Composites Engineering 1994;4:995–1009.